Using Unmanned Multicopter Vehicles for Atmospheric Research and Air Quality Measurement

Monika Scheibe[1], Thomas Wiedemann[2], Klaus Dietl[3]

1 Deutsches Zentrum für Luft- und Raumfahrt (DLR), Institut für Physik der Atmosphäre, Oberpfaffenhofen, Germany

5   2 Deutsches Zentrum für Luft- und Raumfahrt (DLR), Flugbetrieb, Oberpfaffenhofen, Germany

3 Flugsensor, Andechs, Germany

Correspondence to: Monika Scheibe (monika.scheibe@dlr.de)

Abstract. Small UAS have left the status of being pure research objects at university level and they

10   have improved their image as sensor carrier remarkably in the past few years. An industrial sector has risen within few years from toy to aerial movable platforms for service, maintenance and repair. Consequently the use of small multirotor aircraft has become very popular over a wide range of field research (Villa & et al., An Overview of Small Unmanned Aerial Vehicles for Air Quality Measurements: Present Applications and Future Prospectives, 2016). Particularly UAS represent well-

15   established tools for atmospheric research in the boundary layer, studies of human-environmental interaction and surveillance of anthropogenic pollution and hazards. This started up production for small gas and particle sensors within the years (Villa & et al., Development and Validation of a UAV Based System for Air Pollution Measurements, 2016), (Alvarado & et al., 2017), (Chang & et al., 2016; Eu & et al., An Airflow Analysis Study of Quadrotor Based Flying Sniffer Robot, 2014). Therefor a well-

20   known platform is a need to deliver a reliable scientific dataset. Common methods are to characterize its in-flight behavior and the airflow around the platform. These aerodynamic properties are important in order to design and place sensors on UAS and to understand its interaction with the environment. From our knowledge a comprehensive study is still missing (Schuyler & Guzman, 2017). There are different approaches: simulation (Sandstrom, 2017), (Eu & et al., An Airflow Analysis Study of

25   Quadrotor Based Flying Sniffer Robot, 2014) (Eu & Yap, An Exploratory Study Of Quadrotor's Propellers Impact Uusing 3D Gas Dispersion Simulator, 2017) and adaption of full scale helicopter theory to small scale multirotor physics (Wayne, 2000) with considered constant blade pitch. Both aim to broaden the technical and physical understanding of small UAS (Hoffmann & et al., 2007). This work uses the experimental way for an approach to questions concerning airflow and dimension of disturbed

30   atmosphere as well of how long it takes the atmosphere to recover from copter disruption.

While these results are not entirely unexpected, direct experimental confirmation has been elusive so far. Importantly, our results increase confidence in the current understanding of the platform induced influence on a sensor / measurement. Further, we provide guidance on the improvement of placing sensors on a flying platform and present a method for estimating the size of the platforms' influence on the atmosphere.

1 Introduction

Multicopter platforms have become very common to be used as a carrier for gas and particle sensors. They are wide spread available, cheap and easy to handle. Equipped with gas and/or particle sensors they are a powerful tool to gain scientific data about the predominant inhabited part of the atmosphere:
5   the boundary layer. However, the dispersion of the substances of interest is mostly dominated by advection mechanism and airflow. Therefore, it is important to understand the aerodynamic impact of the multicopter's propulsion system on its surrounding.

In this context an essential property of the copter platform is the specific ratio of motor performance and take-off weight. This ratio leads to a derivable relationship of copter-environment interaction. These
10   interactions include well-known aerodynamic effects applied to full-scale helicopters that are until today poorly adopted to small scale vehicles.

This work presents studies about the air volume impacting a copter based gas or particle sensor measurement (section 4.1), the impact of aerodynamic effects on the sensor position (section 4.2) and the time the atmosphere needs to recover from multicopter propulsion system disturbance (section 4.3).
15   Finally, it contains a generalized statement independently of the specific flown multicopter platform. For our investigations we carried out several experiments with different types of multicopter. To evaluate the interaction of the UAV's propulsion system, we made use of smoke grenades in order to get a visual feedback about the disturbance. The finding of the presented work may help to design UAVs in the future for gas or particle sensing application. In the following we will use the expression "copter"
20   as a generic term for multirotor based flying copter platforms independently of the geometrical shape and its number of rotors.

2 Theoretical Background

From helicopter theory the rotor disk generates an area of underpressure directly above it and an area of overpressure right below it. The pressure gradient causes surrounding air accelerating through the rotor
25   disk resulting in an air mass flow which is a function of motor speed. If thrust forces overcome gravity forces the helicopter begins to rise.

Hence for multicopter platforms the rotor disk is more complex as it is consisting of several (even numbered) propulsion systems of which each neighboring propeller is counter-rotating. To make different copter types and configurations, their size and the copters' weight comparable we are looking
30   for characteristic numbers. From different analytical flow studies e.g. (Eu & et al., An Airflow Analysis Study of Quadrotor Based Flying Sniffer Robot, 2014), (Sandstrom, 2017), it is obvious that characteristic numbers which are influenced by a helicopters' rotor disk are not directly transferrable to multicopters. To gain numbered estimates we will replace the rotor disk plane ring element from helicopter theory. In this work we envelop with the term "virtual rotor disk area" all single rotor ring
35   planes of a multicopters' propulsion system.

The mathematically simplest state of a flying copter is the hovering. In this static state the copter's position and height remain constant. Thus no acceleration affects the copter compared to the (far) surrounding air. The flow conditions are widely axisymmetric and are only dependent on propeller radius and propeller pitch. Further the rotational speed of all rotors during hovering is equal. Due to the rotation and pitch angle the rotor blade pushes air from above the rotor disk downwards (direction +z) resulting in a constant mass (air) flow.

By accelerating air in downward direction, the motor produces a thrust F_{T_i} according to momentum conservation law. Since in hovering state the coper is not accelerated, the thrust F_T compensates gravity G (Figure 1**Fehler! Verweisquelle konnte nicht gefunden werden.**). Therefore, a simple approach to estimate the strength of air flow caused by a copter is the momentum theory.
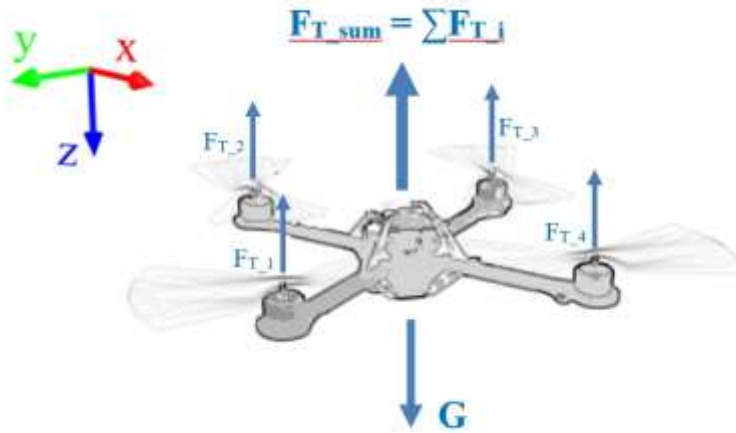

Figure 1 (Far field) forces on a quadrocopter during hover. Schematic for a four--rotor platform.

Momentum conservation law delivers the connection between thrust and mass flow:

$$F_{T_{sum}} = \dot{m} * v_d - \dot{m} * v_u = \rho * A_{sum} * v_d{}^2 \tag{1}$$

$$\text{with } \dot{m} = \rho * A * v_d \tag{2}$$

while $F_{T_{sum}}$ is the sum of thrust forces of all propellers in Newton, $\dot{m}$ = air mass flow in kg/s, v_d is the rotor induced air flow velocity, normal to the disk plane far downstream in m/s (Figure 2), A_{sum} is the virtual rotor disk area, equal to the sum of all single rotor ring planes in m² and ρ is the air density in kg/m³.

Further is assumed that the far upstream air has no velocity $v_u = 0$.

By comparing the work done by the copter in a certain time:

$$P = F_{T\_sum} * v_i,\tag{3}$$

where v_i is the wake-induced velocity at the virtual rotor disk area, with the change of energy in the downstream

$$\Delta E = \frac{1}{2}\dot{m} * v_d^2 - \frac{1}{2}\dot{m} * v_u^2,\tag{4}$$

we can derive:

$$\frac{1}{2}\dot{m} * v_d^2 = \dot{m} * v_d * v_i\tag{5}$$

$$v_d = 2 * v_i\tag{6}$$

Further in hover the gravity forces are compensated by the thrust ($F_{T\_sum} = G$) which leads to:

$$v_{ih} = \sqrt{\frac{G}{2 * \rho * A_{sum}}}\tag{7}$$

(Note: induced velocity is the same as if calculations are proportionate made for only one propeller)
According to that, the airflow is proportional to the force caused by gravity G and therefore is highly depending on the weight of the copter. Further it can be seen, that the size of the rotor blade influences the airflow.
For a multicopter actuator disk all blade disks can be summarized

$$A_{sum} = \Sigma \left(\pi * (r_a^2 - r_i^2) \right)\tag{8}$$
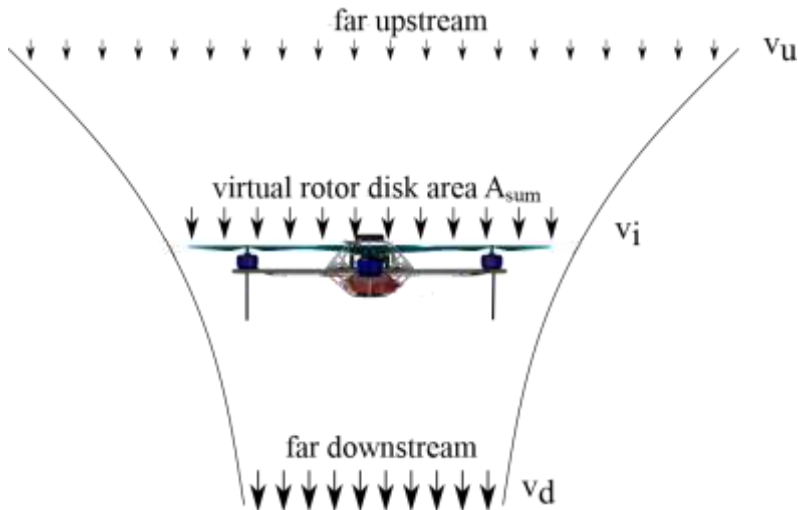
Figure 2 Momentum theory flow model in hover state: mass conservation leads to wake contraction far downstream

Due to the induced flow it is obvious that

5   i)   The air volume contributing to a sensor measurement on a copter platform is not assumable to be a spatial point measurement. Rather, the measurement corresponds to a spatial volume integral.

     ii)   There might be more favoured positions for a sensor than others.

     iii)   Depending on the used platform geometry, its size and propulsion number it takes the
10   atmosphere a specific time to recover from disturbance.

Consequently quantifying and relating the flown platform to the interaction with the environment is an important issue when designing a gas or particle sensing platform, since the disturbance will affect the measurements. A sensor mounted below the rotor disk (z-axes) will be strongly influenced by downwash
15 (thick red line in Figure 3). This will hardly be falsifying measurements of fast sensors, in a well-mixed atmosphere or measurements of a homogeneously distributed gas species. For particle sensors, slow sensors, sniffer robots and in any inhomogeneous expected environment a top mounted sensor is recommended. It makes no big difference where on top the sensor is located except for mountings directly on the copter frame surface if the frame size is a solid plate and represents a noteworthy obstacle
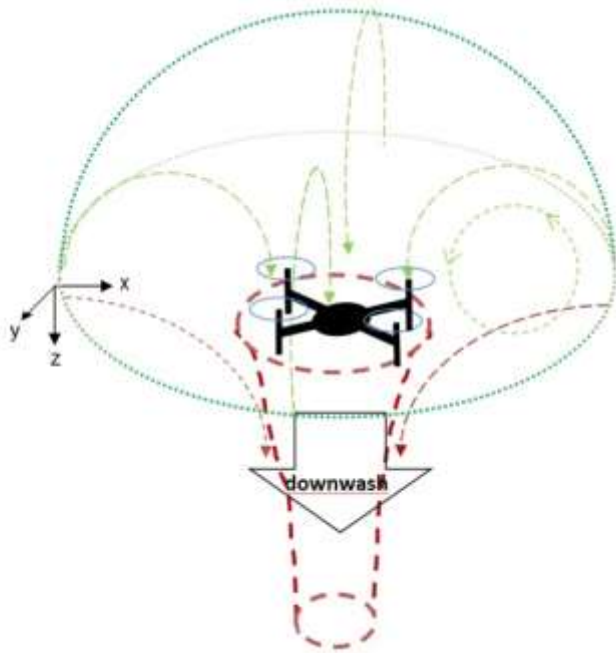20 for the downwash. Then we recommend a mounting on the frame's edge.

Figure 3 Theoretical expected influenced air flow volume by virtual rotor disk area

3 Experimental Validations:

3.1 Limitations of Momentum Theory

Momentum theory concentrates on estimates of induced power at a given thrust. It is not concerned with detailed rotor loads or flow. Hence, it will give us an estimate of the rotor disk induced air velocity. Therefor each single rotor will be considered to be a circle shaped disk without thickness. Basic conservation laws of fluid motion are applied. However, it is only a theoretical approximation of the true airflow and only holds under certain assumptions:

Fluid Assumptions:

- The flow through the rotor behaves as an ideal fluid: quasi-steady, incompressible, frictionless
- Well-defined, smooth slipstream
- The flow is one-dimensional
- The flow is laminar; rotational energy in the wake is neglected.
- The air outside the stream tube remains undisturbed by the virtual rotor disk area.
- The wind velocity is zero: $|W| = 0$.

Technical Assumptions of each single rotor disk:

- The motor disk is even. Angled motor mounts are not satisfied covered (See section 4.2)
- Axial symmetry of the rotor disk
- The radius of a plane perpendicular to the control volume at the rotor disk equals the rotor radius.
- The rotor disk consists of an infinite number of rotor blades. Hence, the aerodynamic forces over the rotor disk are uniform and constant distributed.
- The rotor disk equates an infinitely thin disk and offers no air drag to the passing air
- The flow is laminar and therefore no spinning power is transferred.
- The air outside the streamtube remains undisturbed by the actuator disk.
- Constant blade pitch

However, the question remains: how well does this theory describe the actual interaction of the UAV with it surrounding in reality. Therefore, we carried out some experiments to evaluate the theory.

3.2 Copter Platform

In the experiments we considered different types of multicopters. In particular we were interested in a DJI S900 hexacopter with an E1200 propulsion system as well as an AscTec Hummingbird (quadcopter). Those were examined in different smoke test. Further, for comparison we carried out experiments with small commercial available copters as well as self-build quadcopter and hexacopter configurations. Complementary we added smoke tests found in the literature. An overview of the different platforms in use is given in Table 1.

Table 1 Smoke tested multicopter platforms

Performance Data	AscTec Hummingbird	DJI E1200	T-Drones SMART.H-B Copter	Blade 180 QX	Blade Nano	Tarot680	Airrobot AR100-B[1]
Actual Takeoff Weight/ g	700	6800	1035	0.080	0.019	3255	1300
Number of Motors	4	6	6	4	4	6	4
Motor Power (each) / W	80	700	120			426	
Motor Type	Hacker X-BL 52S (almost cp. to Hacker A20-50S)	DJI 4216-310	Tiger Motor Air Gear 200 (2205-2000)	Blade 8.5 mm brushed motor with pinion	Blade 6 mm brushed motor with pinion	Tiger Motor MN3508-16	
Max. Thrust total / N	20	234	35			15.80	
Weight-to-power Ratio / (g/W)	8.34	7.27	7.58	16.33	4.77	7.99	
Frame Dimensions / mm	540	920	380	292	102	695	1000
Blade Material	Asc Tec flex	Carbon Fiber folding blades	Nylon	Nylon	Nylon	Carbon Fiber	Carbon Fiber
Blade Dimensions / inch	8	17	6.5	5.35	0.	13	
Blade Angle	4.5	6	3.5	2.5		5.5	
Size of Virtual Rotor Disk Area (A_sum / m²)	0.1285	0.7085	0.1223	0.0578	0.0081	0.5338	0.1033
Speed Coefficient (=specific speed) (RPM)/V	1088	310	2000	3000	11000	700	
Battery / mA	2200 (LiPo)	16000 (LiPo)	3300 (LiPo)	500 (LiPo)	175 (LiPo)	10000 (LiPo)	4000 (Lithium Ion)
Number of Battery Cells/Packs	3S1P	6S1P	3S1P	1S1P	1S1P	4S1P	4S1P
Electronic Speed Control	X-BLDC Brushless ESC	DJI E1200 Pro 640X ESC	T-Air 15A	Onboard	Onboard	Hobbywing XRotor 40A-OPTO ESC	
ESC / A	12	40	15 (20 Peak)	5	2	40	

[1] From: (Neumann, 2013)

3.3 Experimental Setup

To understand the air flow around a copter we decided to make it visible with real smoke tests. To avoid wall effects these tests were performed outdoors. In the test the interaction of different copter platforms with smoke was monitored by cameras from different perspectives. From the videos and pictures taken by cameras we estimate the dimensions of disturbances. Weather conditions were chosen to calm days with a cloud cover to approach the zero wind velocity condition as close as possible.

Figure 4 Field smoke test setup September 2017   **Figure 5 Test B Camera positions during smoke test March 2017**

We performed three types of smoke tests with different aims:

Type 1: Smoke test with static copter: In this case the examined copter was fixed on a tripod. Therefore, the copter has no relative velocity to the air, neither in vertical nor in horizontal direction. The motor power during the test was shortly below lift-off to avoid the tripod to vibrate. In the experiment we induced smoke generated with a Björnax AB AX-3 smoke cartridge. The cartridge was manually moved to different positions in the copter surrounding to visualize the airstream around the copter. The experiment was recorded by a camera for later evaluation. (Section 4.1)

Type 2: Smoke test during hover: The aim of the second test type was to determine the dimension of the downwash of the copter's propulsion system and to identify feasible locations for a gas sensor on the copter. Therefore, on a shallow meadow eight GPS located cameras were placed on different heights in a circle formation (approximately 40m diameter). Additionally a camera copter was positioned above the scene downwind aside to observe the scene from an elevated spot. In the centre of the camera circle smoke was released from a smoke bomb. The different copter platforms slowly approached the smoke

plume and stayed in its proximity and the disturbance of the smoke dispersion by the copter was recorded by the cameras from different perspectives. (Section 4.2)

Type 3: Smoke test during slow horizontal flight: In the test the experimental setup was the same as in Type 2 test. In contrast the copters slowly passed the smoke plume with a horizontal velocity. The aim of those tests was to additionally determine the disturbed volume below the rotor disk. Further, based on the recorded videos it was possible to estimate the temporal duration of the perturbation, in other words: the recovery time of the smoke plume after an overflight (Section 4.3)

4 Results

4.1 Intake Area and Volume

Tests of type 1 were performed in May, and October 2017. The first test was with the T-Drones Copter (hexacopter) being horizontally mounted on a tripod 150 cm above ground. The second tests with the Blade Nano fixed the same way. Motor power during the tests was shortly below lift off to avoid the tripod to vibrate. Smoke from a Björnax AB AX-3 smoke cartridge was induced primarily from left side of view of Figure 6 and Figure 7 (T-Drones). Wind condition was almost calm. Two video sequences where taken during two tests by a Canon Powershot 12 Camera in 1024x768 pixel resolution and 30 frames per second (fps). Afterwards smoke plume trajectories were identified from video with the software „Tracker" V4.97 by Douglas Brown; Tracker is a free video analysis and modeling tool built on the Open Source Physics (OSP) Java framework (Brown, 2017).

Identification of tracks was made by marking a peculiar target like a stable eddy or a point of obvious stable smoke density and following its way. Evolution rate was set to 20 % to be sure to match the same object in the next frame. Automark level was set to 4. This trajectory marking occurred half automated by the software's implemented algorithms, half manually by eye. Trajectories of each side are mirrored on the opposite side of the vertical copter axis as motors are assumed to behave symmetrically during no-wind conditions in hover state. Different colors were chosen to separate different trajectories.

Trajectories starting from above the rotor disk usually were accelerated and deflected into axial flow through the rotor disk. Trajectories starting from below the rotor disk usually stayed below the rotor disk. They were attracted by the slipstream towards a point below the copter center and were finally deflected downwards. Slipstream length was not documented in this test.
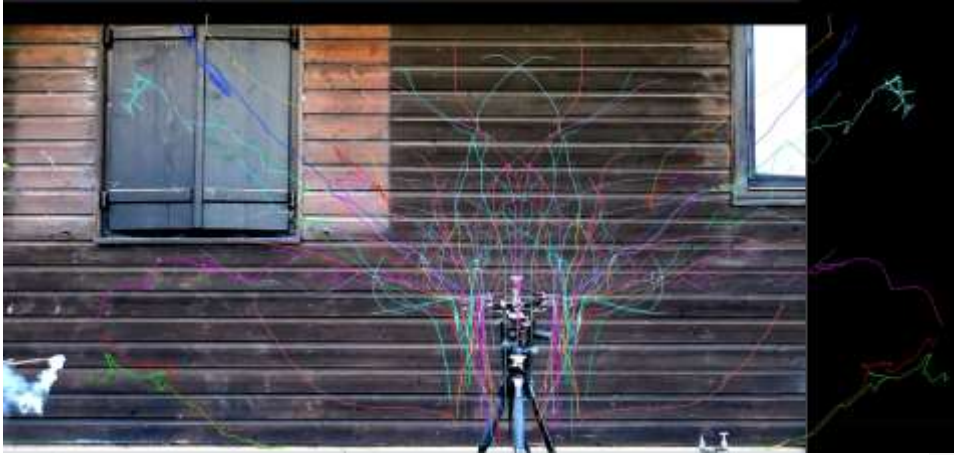
Figure 6 Smoke trajectories (mirrored each side)

Abstracted trajectories around the copter indicate an observed volume dimension of around six times the virtual rotor disk area diameter in horizontal and around two times the virtual rotor disk area diameter in the vertical. The shape of the observed volume equals more a closed torus than the expected hemisphere (Figure 3).
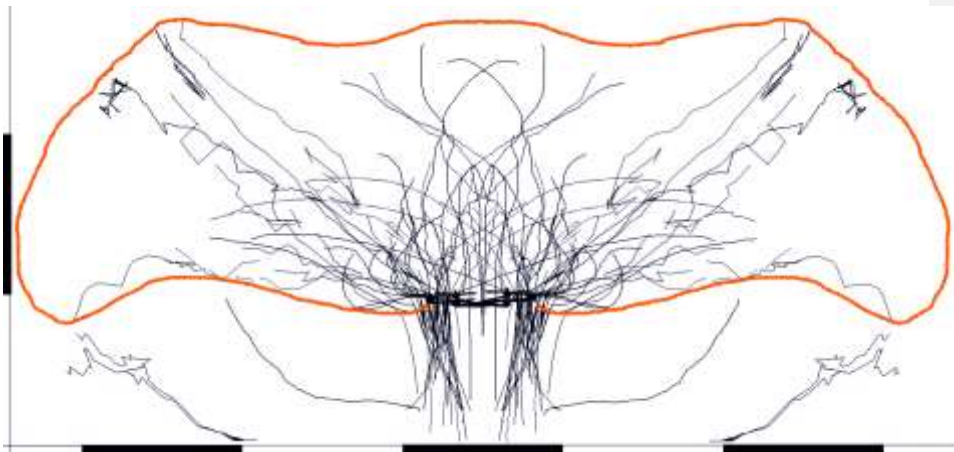

Figure 7 Abstracted Trajectories and observed area of influence

Roughly estimating the volume V_o with two cones nested within an elliptical-shaped torus with the adjusted torus formula
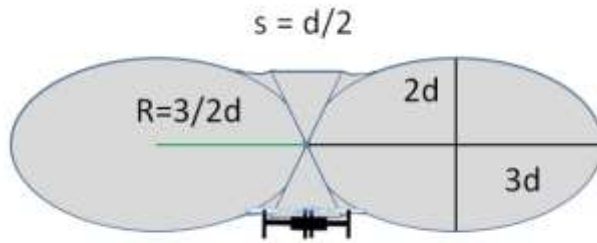
Figure 8 Cross-section trough the torus shaped sucked volume

$$V_\circ = 2 \pi R * \frac{2d*3d*\pi}{4} + 2[V_{cone}] \tag{9}$$

with R being the path length of the center of area (rule of Guldin)

$$V_\circ = 2 * \left(\frac{3}{2} * d\right) * \frac{6}{4} * d^2 * \pi^2 + 2 * \left[\frac{1}{3} d \pi \left(\frac{d}{2}\right)^2\right] \tag{10}$$

$$V_\circ = \frac{9}{2} d^3 * \pi^2 + 2 * \left[\frac{1}{3} * d * \pi * \frac{d^2}{4}\right] \tag{11}$$

$$V_\circ = \frac{9}{2} d^3 * \pi^2 + \frac{1}{6} * d^3 * \pi \tag{12}$$

Table 2 Estimated Intake Volumes for The Different Copters

Copter name	AScTec Humming bird	DJI E1200 (S900 frame)	T-Drones SMART.H-B Copter	Blade 180 QX	Blade Nano	Tarot680	Airrobot AR100-B
Copter type	Quadrocopter	Hexacopter	Hexacopter	Quadrocopter	Quadrocopter	Hexacopter	Quadrocopter
Diameter of rotor disc area / m	1.352	0.743	0.545	0.355	0.151	1.024	0.722
Estimated from above sucked Volume / m³	111.0	18.4	7.3	2.0	0.2	48.3	16.9

4.2 Vertical and Horizontal Dimension of Disturbances

The horizontal disruption caused by DJI E1200 was found to be around four times the rotor disk and the vertical disturbance was observed to be larger than nine times the dimension of the rotor disk.

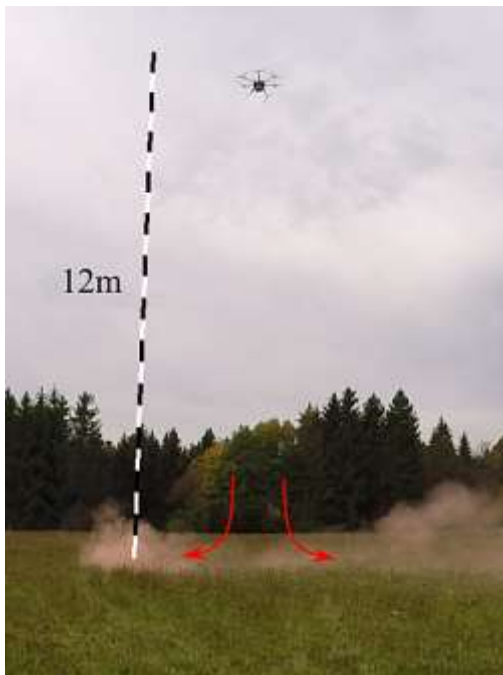**Figure 9 DJI E1200 Horizontal Atmospheric Disturbance**

Figure 10 Vertical Disturbance DJI E1200

For the Humming Bird quadrocopter we observed horizontal disruptions of about vertical disturbance of the of about eight times of the dimension of the rotor disk.
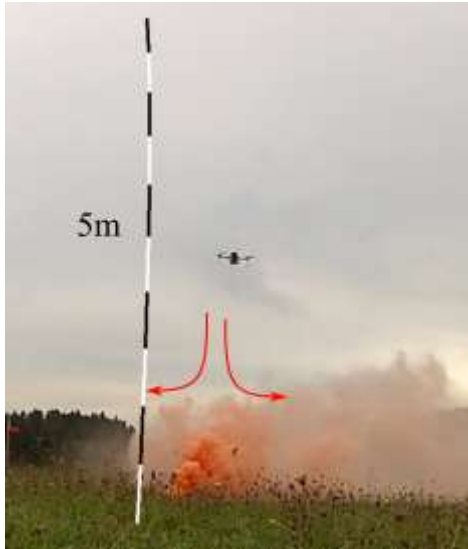
Figure 11 Humming Bird horizontal disturbance

Figure 12 Vertical disturbance Humming Bird

There are two main influences on the spatial dimension of atmospheric disturbance: On the one hand side the copter with the slowest motor rotary speed in hover showed the largest spatial disturbance of the surrounding atmosphere. On the other side the copter with the smallest weight to total propulsion disk ratio showed the largest disturbance. We observed that a dihedral motor mount might not only contribute to a more stable flight. There are hints that the motor induced perturbation spreads over a larger plane. Hence, the widened impulse results in a smaller vertical motor induced influence which also seems to disappear earlier.

Table 3 Disturbance Comparison

Copter name	AScTec Humming bird	DJI E1200 (S900 frame)	T-Drones SMART.H-B Copter	Blade 180 QX	Blade Nano	Tarot680	Airrobot AR100-B[2]
Copter type	Quadrocopter	Hexacopter	Hexacopter	Quadrocopter	Quadrocopter	Hexacopter	Quadrocopter
Take-off weight / g	700	6800	1035	80	19	3255	1300
Rotary speed hover / RPM	5315	3499	8110	4274	20246	3897	
Single rotor disk plane (SDP) / m²	0.0321	0.1181	0.0204	0.0144	0.0020	0.0890	0.0258
Size of virtual rotor disk area (A_sum / m²) (VRA)	0.1285	0.7085	0.1223	0.0578	0.0081	0.5338	0.1033
Weight to VRA per frame span ratio kg / m²	2.94	8.83	3.21	0.30	0.25	4.19	6.79
Horizontal disturbance / x-times diameter	2.2	4.0	6.0	2.8	3.2	5.0	7.65
Vertical disturbance above rotor disk / x-times diameter	2	1.5	2				> 2
Downwash disturbance / x-times diameter	8.0	9.2	9.6	2.4	9.6	23.4	14.7

---

[2] From: (Neumann, 2013)

Withal simplified examination of momentum theory from our smoke tests we find a good estimate of a relationship. The vertical dimension of a copters atmospheric disturbance is linear proportional to the root of thrust and take-off weight per total lift area:

$$S \sim \sqrt{\frac{T*m}{A}}$$
(13)

with

S - dimension of disturbance x-times diameter rotor disk area; dimensionless

T - thrust in N

m - take-off weight (total mass) in kg

A - total lift area of all rotor disks (sum) in m²

The corresponding images and videos that led to this result for the different copter platforms can be found in the addendum.

Table 4 shows a summary.

With that simplified correlation an estimation of the vertical disturbance dimension can be made (blue line in Figure 13). The only discrepancy we found is for very small platforms (Blade Nano QX) and for platforms with dihedral motor design (DJI E1200 / S900).

The mean horizontal disturbance was found to be in the size of four times the rotor disk area (orange line):
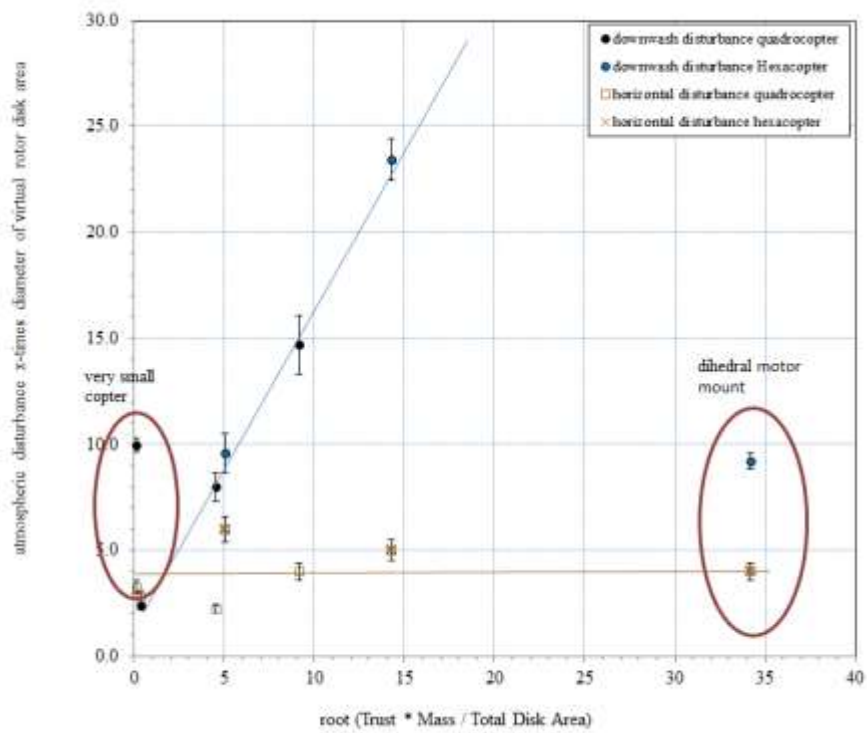
Figure 13 Relationship between atmospheric disturbance and copter parameters (thrust, mass and lift area)

Table 4

Copter name	AScTec Hummingbird	DJI E1200 (S900 frame)	T-Drones SMART.H-B Copter	Blade 180 QX	Blade Nano	Tarot680	Airrobot AR100-B[3]
Copter type	Quadrocopter	Hexacopter	Hexacopter	Quadrocopter	Quadrocopter	Hexacopter	Quadrocopter
Downwash disturbance / x-times diameter S	8.0	9.2	9.6	2.4	9.6	23.4	14.7
$\sqrt{\dfrac{T * m}{A}}$	4.546	34.204	5.052	0.370	0.112	14.290	9.148

[3] From: (Neumann, 2013)

4.3 Temporal duration of perturbation

Typical copter based field measurements take place in the lowest 200 to 300 m of the atmosphere during daylight. They do mostly not extend 30 minutes of flight time in a row. Here, from a micrometeorological point of view, typical orders of natural wind and turbulence velocities are in the order of meters for space and seconds to a few minutes for time. Especially vertical kinetic movements are even smaller in most cases, except for thermic activity caused by solar radiation. Natural generated kinetic turbulence wakes have in common that their energy dissipates with time, their altitude and surrounding roughness. The smaller the turbulence wakes the less intrinsic energy they provide to keep themselves alive (Stull, 1988).

Figure 14 shows an example of a typical wind profile of atmospheric layering in the above-mentioned heights (grey and black). It furthermore shows an example of downwash drift. This figure makes obvious that, depending on the flight level, the induced turbulence will be blown more or less lateral depending on the wind velocity at this altitude. Hence, a lower flight disturbs the air directly below the platform, a flight at a higher altitude disturbs the air lateral to the platform.
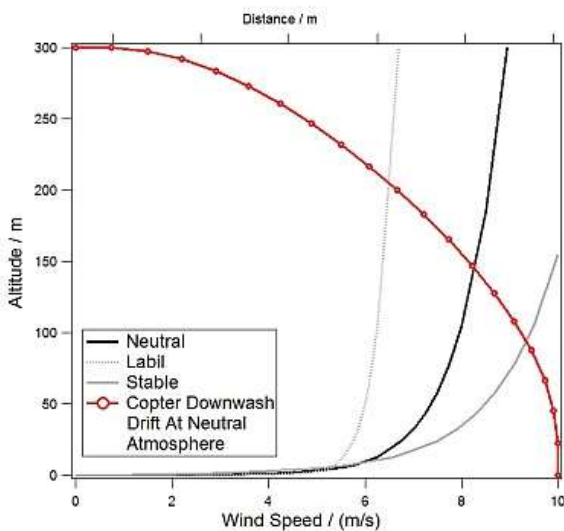

Figure 14 Typical Variations of Horizontal Wind Speed and Example Downwash Drift with Altitude

In summary it turned out that the time the atmosphere needs to recover from a highly turbulent disturbed state back to ambient flow state depends of two parameters: On the one hand side is the intensity of the copter induced turbulence –depending on actual motor power- on the other side the natural horizontal wind velocity and the natural atmospheric turbulence. The larger the natural horizontal wind velocity (advection) and the larger and energetic the natural convection the faster the recovery to original flow state.

The time the smoke -and thus atmosphere- needed to recover from a propulsion disturbance according to our videos was found to be 3 to 5 seconds for all copters. In these video sequences the slow copter overpasses where at low altitudes of only a few meters above the ground. Further disturbance depth where not studied during these tests. Obviously the propulsion system does not influence this time span. Of course the dimension size of the disturbance differed according to the propulsion's energetic impulse. The larger slow rotating propulsion platforms left larger but slower eddies than the copters with smaller and faster rotating propulsions.

4.4 Considering Energetic Influence of a Copter's Propulsion System

Due to the strong vertical wind component in a typical order of 2 to 10 m/s a copter downwash adds kinetic energy to the surrounding air. In this section we estimate its energetic influence on physical parameters' measurement.

Assuming air being moved adiabatic results in changes of the turbulent heat flux: the downward moved air has a different temperature than the surrounding air.

In the following a calculation example for a hovering DJI E1200 where a temperature sensor is mounted 0.5 m below the rotor disk area.

Copter start altitude: 650 m above mean sea level (MSL); hover flight altitude: 100 m above ground level (AGL)

Temperature at start altitude: 10 °C

Induced downwash velocity at copter height: -6.14 m/s (negative as downward faced)

Assumptions: no horizontal wind, no natural turbulence, no convection

The downwash induced vertical turbulence kinetic energy (TKE) per unit mass (m) of the copter rotor is:

$TKE / m = 0.5 * w^2 = 0.5 * (-6.14)^2 = 18.8 \ m^2/s^2$

This is about one magnitude larger than typical natural turbulence TKE/m values.

Further assumptions:

Temperature gradient according to dry adiabatic lapse rate: 0.98 K / 100 m

Vertical rotor influence during hover for DJI E1200 was found to be 1.5 times the rotor disk area, results in a total distance between sucked air and sensor position (2.03 + 0.5) m = 2.53 m

Maximum difference between sucked surrounding air and measured temperature at sensor level is -0.025 K as the downward moved air is colder than the surrounding air -what might be far away from most to be used temperature sensors accuracy.

Estimating the hovering DJI E1200's contribution to vertical (kinematic) heat flux per unit mass, which is the change of vertical velocity (w) times the change of virtual temperature (θ), results in w * θ = -6.5 m/s *

(-0.00015) K = 0.001 K m/s; A minimal positive heat flux, that is three orders smaller than natural vertical kinematic eddy heat fluxes and can be neglected.

5 Discussion and Conclusion

In this work we showed that the position of a sensor on a copter platform might influence its ability for representative gas and particle measurement. The sensor position impacts the amount of "new" air seen by the sensor. It impacts the air volume that passes the sensor during a measurement interval and about which the measurement has to be to be integrated. Strictly speaking the measurement volume has to be weighted by distance of the copter center due to different acceleration of the air stream in this volume.

Also, a multicopter induced turbulent airflow mixes air from above with a different temperature level to lower altitude. This influences not only temperature measurements but also humidity and thereby air density and mixing ratios of gas species.

There might be solutions like booms and tethered sensors hanging far down the copter. All these solutions easily lead to instable flight conditions, like vibration (booms) or pendulum swinging (tethered weight).

The far best solution for an undisturbed basic research of gases and particles for moved measurements is a fixed wing with one (or more) pusher motor(s). As these measurements often take place in harsh environment without well prepared runway available a VTOL (vertical take-off and landing) might be a compromise. The advantage of a fixed wing of larger payloads and extended flight duration meet requirements of vertical take-off and landing abilities. However propeller blades that are optimized primarily for a vertical operation cannot compete with solely fixed wing propeller blade shapes concerning effectiveness.

Fixed wings are not as agile as copters are and are not able to hover above a spot. Potential benefit of each sensor carrier has to be weighed against any disadvantage on any individual case considering the aims of a measurement.

In general it can be said that due to the compressed state of the air below the rotor disc area it obviously makes sense to mount sensors for temperature, humidity, pressure and inhomogeneous distributed gases as well as for particles on top of the platform, best slightly elevated above the rotor disk area. Temperature sensors mounted above should be protected from direct solar irradiation. Due to thermodynamic theory temperature measurement taken in the compressed regime below rotor disc area is expected to be slightly elevated. Elevated temperature results in lower relative humidity measurement.

References

Alphasense Ltd. (December 2015). *Alphasense User Manual OPC-N2 Optical Particle Counter 072-0300(Issue 5)*. Essex.CM77 7AA. UK.

Alvarado, M., & et al. (February 2017). A Methodology to Monitor Airborne PM10 Dust Particles Using a Small Unmanned Aerial Vehicle. *Sensors 2017*.

Bangura, M., & et al. (January 2016). Aerodynamics of Rotor Blades for Quadrotors.

Brown, D. (18. 06 2017). *Tracker Video Analysis and Modeling Tool for Physics Education*. (Douglas Brown) Abgerufen am 10. 07 2017 von http://physlets.org/tracker/

Chang, C.-C., & et al. (2016). Development of a multicopter-carried whole air sampling apparatus and its applications in environmental studies. *Chemosphere, 144*, S. 484–492.

Eu, K., & et al. (04. 07 2014). An Airflow Analysis Study of Quadrotor Based Flying Sniffer Robot. *Applied Mechanics and Materials*(Vol. 627), S. 246-250.

Eu, K., & Yap, K. (2017). An Exploratory Study Of Quadrotor's Propellers Impact Uusing 3D Gas Dispersion Simulator. In I. o. IEEE (Hrsg.)., (S. 104-106).

Hoffmann, G. M., & et al. (2007). *Quadrotor Helicopter Flight Dynamics and Control:*. AIAA Guidance, Navigation and Control Conference and Exhibit.

Neumann, P. P. (March 2013). Gas Source Localization and Gas Distribution Mapping with a Micro-Drone. *Dissertation*, 34. (F. M. Informatik, Hrsg.) Berlin: Freie Universität Berlin.

Sandstrom, T. (11. January 2017). *Exploring Drone Aerodynamics with Computers*. (NASA) Abgerufen am 28. June 2017 von National Aeronautics and Space Administration: https://www.nasa.gov/image-feature/ames/exploring-drone-aerodynamics-with-computers

Schuyler, T. J., & Guzman, M. I. (23. October 2017). Unmanned Aerial Systems for Monitoring Trace Tropospheric Gases. (MDPI, Hrsg.) *atmosphere, 8*(206), S. 1-16.

Stull, R. B. (1988). *An Introduction to Boundary Layer meteorology*. Dordrecht: Kluwer Academic Publishers.

van der Wall, B. (2015). *Grundlagen der Hubschrauber-Aerodynamik*.

Villa, T. F., & et al. (2016, July). An Overview of Small Unmanned Aerial Vehicles for Air Quality Measurements: Present Applications and Future Prospectives. *Sensors, 16, 1072*.

Villa, T. F., & et al. (December 2016). Development and Validation of a UAV Based System for Air Pollution Measurements. *Sensors, 16, 2202*.

Wayne, J. (2000). *Helicopter Theory* (Revised ed. (1. Januar 2000) Ausg.). Dover Publications.